

Correlation between molecular structure and optical properties for the bis(2-(2-hydroxyphenyl)benzothiazolate) complexes

Xu Huixia^{a,b,*}, Xu Bingshe^{a,b,*}, Fang Xiaohong^{a,c}, Chen Liuqing^{a,b}, Wang Hua^a, Hao Yuying^a

^a Key Laboratory of Interface Science and Engineering in Advanced Materials, Taiyuan University of Technology, Ministry of Education, Shanxi 030024, China

^b College of Materials Science and Engineering, Taiyuan University of Technology, Shanxi 030024, China

^c College of Mining Engineering, Taiyuan University of Technology, Shanxi 030024, China

ARTICLE INFO

Article history:

Received 3 March 2010

Received in revised form 4 September 2010

Accepted 29 September 2010

Available online 8 October 2010

Keywords:

Bis(2-(*n*-methyl-2-hydroxyphenyl)benzothiazolate) complex

Molecular structure

Electroluminescence

ABSTRACT

A series of methyl-substituted bis(2-(hydroxyphenyl)benzothiazolate)zinc derivatives [Zn(*n*-MeBTZ)₂, *n* = 3 (**1a**), 4 (**1b**), 5 (**1c**)] were synthesized to investigate the correlation between molecular structures and optical properties. The results indicate that the blue-emitting ($\lambda_{\text{max}} = 470$ nm) complex **1b** is monomer with a higher PL quantum efficiency than complexes **1a**, **1c**. Two green-emitting ($\lambda_{\text{max}} = 507$ nm and 499 nm) complexes **1a** and **1c** have special bi-molecular structures. The molecular structure for Zn(BTZ)₂ (complex **1**) is dimer. Bilayer organic light-emitting devices were fabricated by using these complexes as emitting layer. The maximum emission wavelengths of the devices are in the range of 501–553 nm. The devices show turn-on voltages at 9.2, 12.7, 2.3 and 10.7 V for complex **1**, **1a**, **1b**, and **1c**, respectively. In particular, the device with complex **1b** shows a higher brightness than the other complexes under the same conditions.

© 2010 Elsevier B.V. All rights reserved.

1. Introduction

Organic light emitting diodes (OLEDs) are primarily prepared with either small molecules or polymer [1–4]. Small molecules have plenty of advantages in that they can be highly purified, vacuum deposited in multilayer stacks, with long display lifetime and high light efficiency. Luminescent metal complexes among small molecules are currently of great interest because of their various applications in photochemistry, OLEDs, and chemical sensors. Zinc complexes have been regarded as excellent emitting materials owing to their ability to achieve high luminescence, as well as good electron transport properties [5–7].

It is well known that Zn(BTZ)₂ is one of the best white electroluminescent materials [8–10]. Zn(BTZ)₂ has been investigated, including substitution of metal ion with other bivalent metal ions [11,12]. However, experimental and theoretical analysis of the correlation between molecular structures and performance of zinc complexes in OLED is rare to date. In this paper, with the assistance of X-ray single-crystal diffraction, the molecular and chemical structures of BTZ complexes were investigated.

A remarkable influences on molecular structures and properties were observed by introduction of methyl as substituent group.

Although blue-emitting materials have been an active research field, blue-light-emitting metal complexes with excellent performance are still rare. It has been shown that some d¹⁰ metal complexes with N, O-donor ligands may have high glass transition temperatures required for stable blue-light OLEDs [13]. In this paper, a series of Zn(*n*-MeBTZ)₂ complexes (Zn(*n*-MeBTZ)₂ = bis(2-(*n*-methyl-2-hydroxyphenyl) benzothiazolate) zinc, *n* = 3 (**1a**), 4 (**1b**), 5 (**1c**)) were synthesized. The maximum emission wavelength of thin film of complex **1b** at room temperature is 470 nm, which is excellent for blue-emitting material. Molecular structures of all complexes and performances (such as thermal stability, photo-physical and electroluminescent properties) were investigated in detail. The chemical structures of complexes **1–1c** are presented in Fig. 1.

2. Experimental

2.1. Materials and instruments

All materials were purified by high-vacuum gradient-temperature sublimation before analysis. C, H, and N microanalysis were carried out with an Elemental Vario EL Elemental analyzer. ¹H NMR data were recorded with Switzerland Bruker DR × 300 NMR spectrometers. FT-IR spectra were determined with a Nicolet

* Corresponding authors at: Key Laboratory of Interface Science and Engineering in Advanced Materials, Taiyuan University of Technology, Ministry of Education, Shanxi 030024, China. Tel.: +86 0351 6014852; fax: +86 0351 6010311.

E-mail addresses: xuhuixia0824@163.com (X. Huixia), xubs@tyut.edu.cn (X. Bingshe).

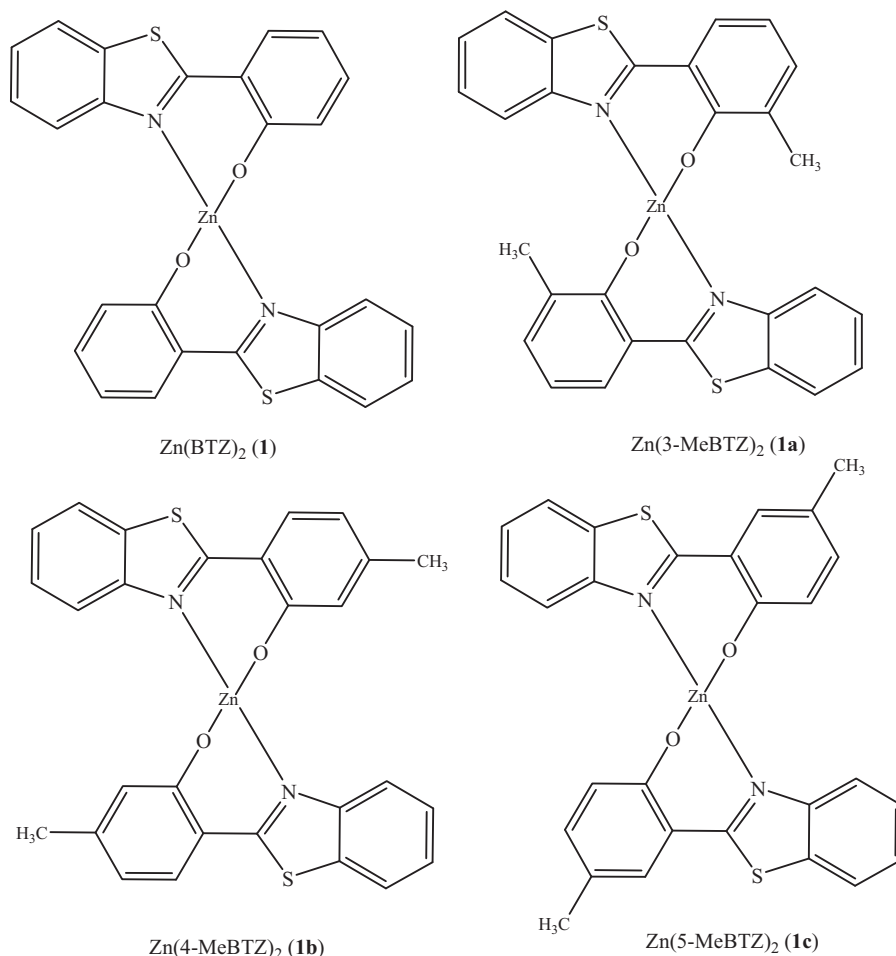


Fig. 1. The chemical structures of all Zn complexes in this study.

7199B spectrometer. Thermal analysis was conducted using STA 409PC thermogravimeter under dry argon atmosphere. Melting points (T_m) of the complexes were determined by differential scanning calorimeter (DSC). UV-vis absorption spectra were recorded by Lambda Bio 40, American PE Co. The photoluminescent (PL)

and electroluminescent (EL) spectra were measured by SPR-920D spectrofluorometer. The fluorescence spectra were examined by Cary Eclipse fluorescence spectrophotometer. The lifetimes (τ_F) in tetrahydrofuran (THF) solution were determined with Edinburgh Analytical Instruments FL900.

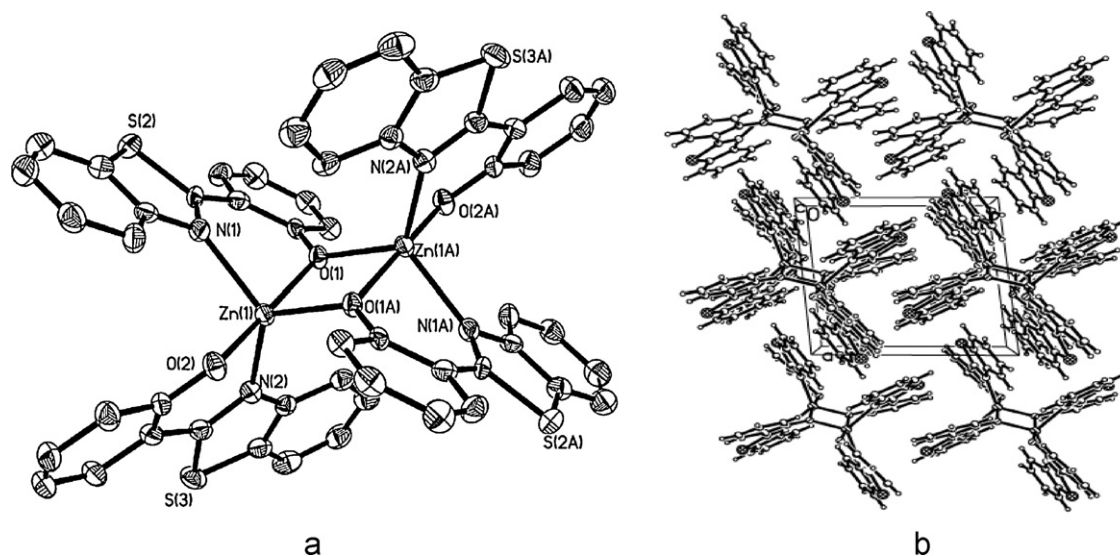


Fig. 2. (a) Molecular structure; (b) crystal diagram between two adjacent molecules of complex 1.

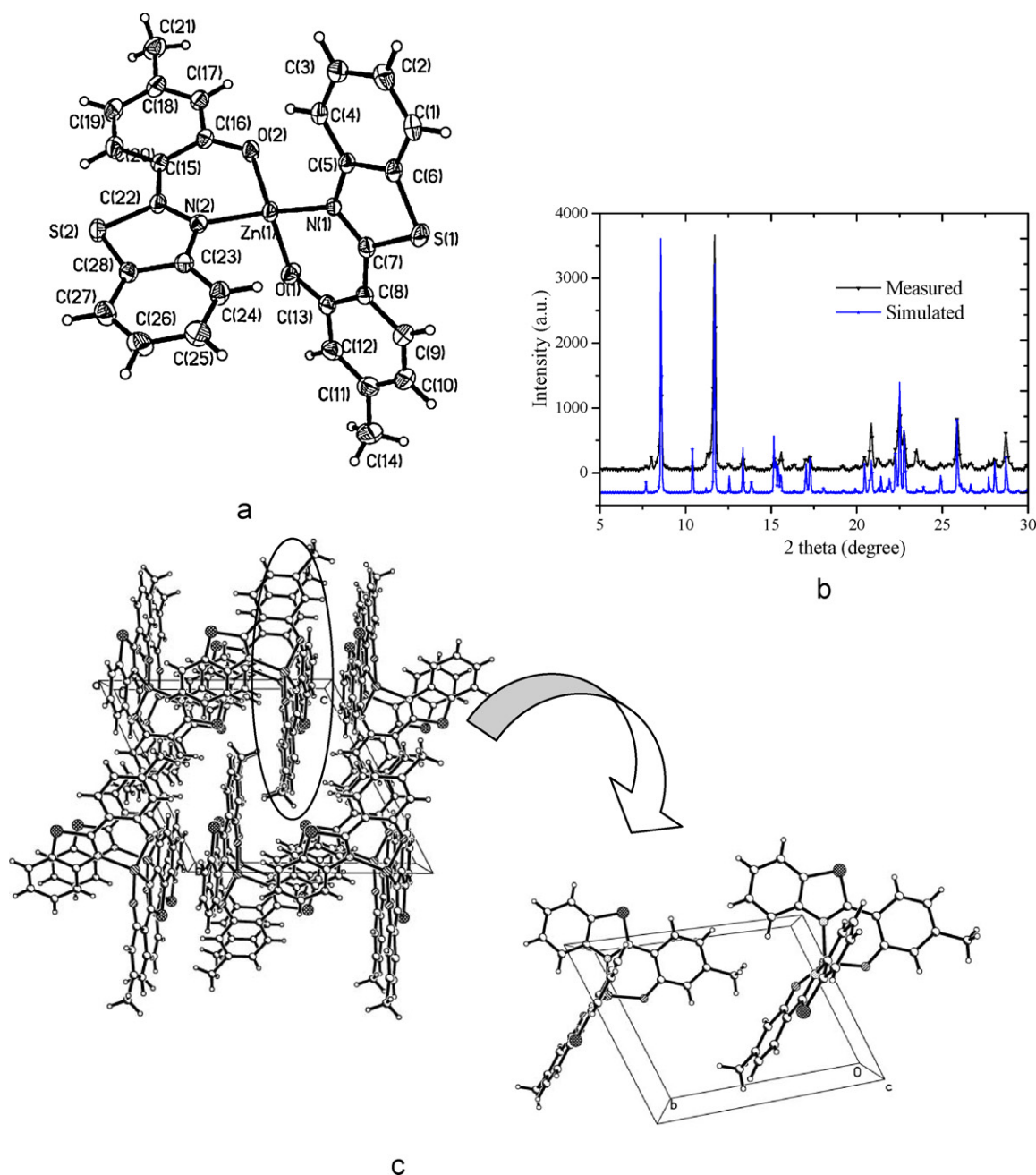


Fig. 3. (a) Molecular structure of complex **1b**; (b) the XRD patterns of complex **1b**; (c) crystal diagram between adjacent molecules of complex **1b** along *c* axis.

Quantum efficiency measurements were carried out at room temperature in THF solution. $\text{Zn}(\text{BTZ})_2$ was used as reference. The concentrations of sample were carefully adjusted so that the optical densities at the intersection of spectra between sample and reference (excitation wavelength) were <0.1 absorption units. PL quantum efficiency were calculated relative to the value of $\text{Zn}(\text{BTZ})_2$ (complex **1**) in THF (set to 1). The equation

$$\Phi_s = \Phi_r \left(\frac{\eta_s^2 A_r I_s}{\eta_r^2 A_s I_r} \right)$$

was used to calculate quantum efficiency, where Φ is the quantum efficiency, η is the refractive index of solution, A is the absorbance at the wavelength of excitation, I is the integrated areas of emission bands, and the subscripts *s* and *r* stand for sample and reference, respectively.

Cyclic voltammetry was performed with Autolab/PG STAT302 in a one-compartment electrolysis cell consisting of a platinum wire as working electrode, a platinum electrode as counter, and a calomel electrode as reference. The solution of 0.1 M TBAPF₆ was used as electrolyte. Cyclic voltammetric behaviors were monitored at scan rate of 50 mV/s.

All the calculations were performed using the density functional theory (DFT) with the Dmol3 program [14]. The geometry optimization was carried out on the DND basis set for all atoms and GGA level. The powder XRD was simulated by the Reflex module of material studio.

The OLED structures employed in this study were double layer. Organic layer was fabricated by high-vacuum (10^{-4} Pa) thermal evaporation onto a glass substrate precoated with an indium–tin-oxide (ITO) layer. Prior to use, the ITO surface was ultrasonicated in a detergent followed by deionized water rinse and dip into acetone.

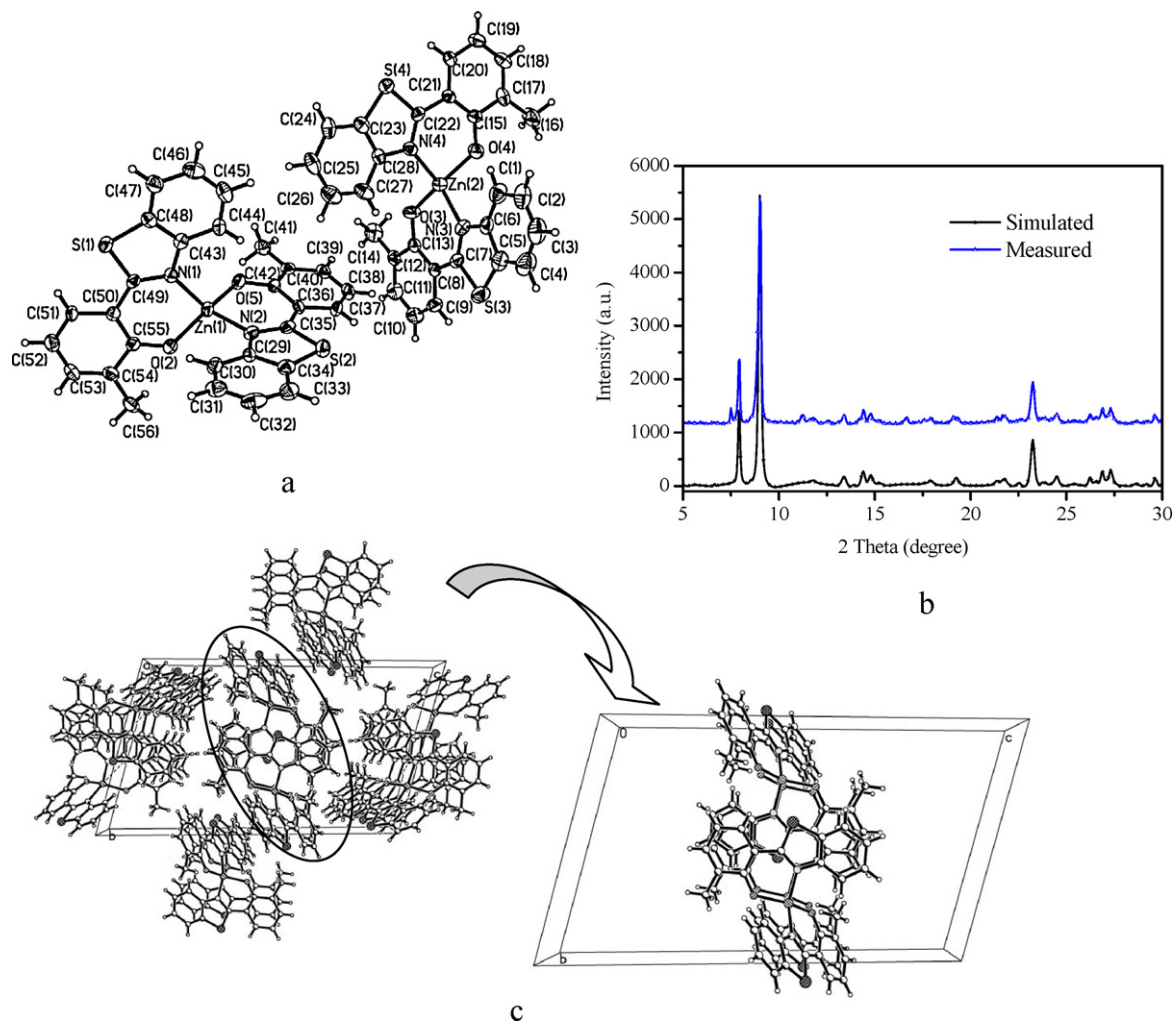


Fig. 4. (a) Molecular structure of complex **1a**; (b) the XRD patterns of complex **1a**; (c) crystal diagram between adjacent molecules of complex **1a** along *b* axis.

Luminance-current-voltage characteristics of OLED were recorded on Keithley 2400 Source Meter and L-2188 spot Brightness Meter.

The single crystals of complexes **1** and **1a–1c** were grown by vacuum sublimation at 390, 390, 415 and 395 °C for 5 h, respec-

tively and collected at room temperature. They were measured on SMART APEX CCD diffractometer, Mo K α ($\lambda = 0.71073 \text{ \AA}$). Cell constants and an orientation matrix for data collections were obtained by Full-matrix least-squares on F^2 . The structures were solved

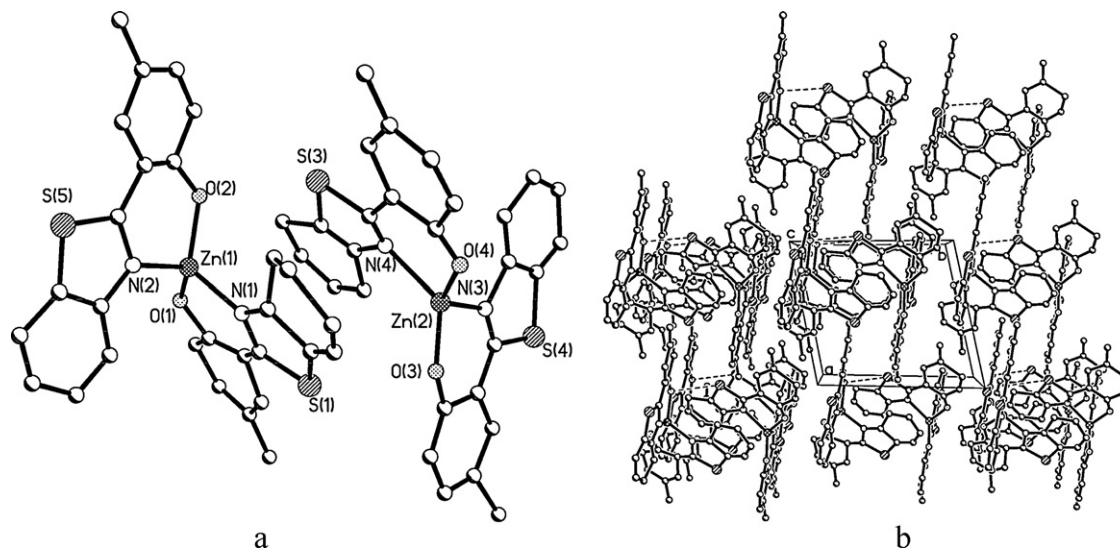


Fig. 5. (a) Molecular structure of complex **1c**; (b) the intermolecular interactions in the solid state of complex **1c** along *c* axis.

by direct methods with SHELXL-97. The powder X-ray diffraction (XRD) spectra were measured by Rigaku D/max 2500.

2.2. Preparation of the ligands

BTZ was synthesized by the reaction of 2-aminobenzenethiol and salicylic acid. The methyl-substituted ligands were obtained from the reaction between 2-aminobenzenethiol and corresponding *n*-methyl salicylic acid in toluene solution. At last, the final products were purified by vacuum sublimation, and product yields were 75–85%.

2-(2-Hydroxyphenyl)benzothiazolate (BTZ): ^1H NMR (300 MHz, CDCl_3): δ 6.99(1H, d), 7.14(1H, m), 7.45(1H, d), 7.5(1H, d), 7.7(2H, m), 7.9(1H, d), 8.02(1H, d), 12.5(1H, s). FT-IR (KBr) cm^{-1} : 3056, 2833, 2595, 1622, 1588, 1482, 1437, 1272, 1250, 1218, 1151, 1129, 970, 862, 757.

2-(3-Methyl-2-hydroxyphenyl)benzothiazolate (3-MeBTZ): ^1H NMR (300 MHz, CDCl_3): δ 2.357(3H, s), 7.037–6.933(1H, s), 7.271–7.201(3H, m), 7.536–7.439(1H, m), 7.933–7.793(1H, m), 8.010–7.982(1H, d), 12.334(1H, s); Anal. calcd for $\text{C}_{14}\text{H}_{11}\text{NOS}$: C, 69.68; H, 4.59; N, 5.80; found: C, 70.76; H, 5.365; N, 5.307; FT-IR (KBr) cm^{-1} : 3054, 2915, 2855, 2350, 1618, 1506, 1438, 1242, 1085, 761, 628.

2-(4-Methyl-2-hydroxyphenyl)benzothiazolate (4-MeBTZ): ^1H NMR (300 MHz, CDCl_3): δ 2.148–2.361(3H, s), 6.745–6.772(1H, d), 6.907(1H, s), 7.348–7.399(1H, m), 7.452–7.503(1H, m), 7.540–7.567(1H, m), 7.857–7.883(1H, d), 7.933–7.960 (1H, d), 12.471(1H, s). Anal. calcd for $\text{C}_{14}\text{H}_{11}\text{NOS}$: C, 69.68; H, 4.59; N, 5.80; found: C, 68.92; H, 4.613; N, 5.690; FT-IR (KBr) cm^{-1} : 3063, 2916, 2855, 1628, 1576, 1482, 1439, 1275, 1242, 1221, 1134, 978, 808, 755.

2-(5-Methyl-2-hydroxyphenyl)benzothiazolate (5-MeBTZ): ^1H NMR (300 MHz, CDCl_3): δ 2.359(3H, s), 6.996–6.7024(1H, d), 7.182–7.212(1H, d), 7.405–7.431(2H, m), 7.479–7.505(1H, d), 7.891–7.919(1H, d), 7.971–7.994(1H, d), 12.331(1H, s). Anal. calcd for $\text{C}_{14}\text{H}_{11}\text{NOS}$: C, 69.68; H, 4.59; N, 5.80; found: C, 70.56; H, 4.49; N, 5.276; FT-IR (KBr) cm^{-1} : 3442, 2921, 2360, 1624, 1594, 1497, 1438, 1274, 1222, 984, 828, 724.

2.3. Preparation of zinc complexes

Bis(2-(3-methyl-2-hydroxyphenyl)benzothiazolate)zinc (**1a**) ($\text{Zn}(3\text{-MeBTZ})_2$): $\text{Zn}(3\text{-MeBTZ})_2$ was synthesized from the reaction between 3-MeBTZ and $\text{Zn}(\text{CH}_3\text{COO})_2 \cdot 2\text{H}_2\text{O}$ in methanol solution. The mixed solution was heated in reflux and stirred for 2 h. The yellow powder was filtered and purified by vacuum sublimation. ^1H NMR (300 MHz, DMSO): δ 1.902(6H, s), 6.488(4H, d), 7.137(2H, s), 7.408–7.527(4H, m), 8.062(2H, d), 8.273(2H, d); MALDI-TOF m/z : $[\text{MH}^+]$ calcd for $\text{C}_{28}\text{H}_{20}\text{N}_2\text{O}_2\text{S}_2\text{Zn}$, 544.03; found: 545.3; Anal. calcd for $\text{C}_{28}\text{H}_{20}\text{N}_2\text{O}_2\text{S}_2\text{Zn}$: C, 61.59; H, 3.69; N, 5.13; found: C, 61.40; H, 3.70; N, 5.12; FT-IR (KBr) cm^{-1} : 3043, 2926, 1653, 1458, 1412, 1225, 1088, 897, 750.

Bis(2-(4-methyl-2-hydroxyphenyl)benzothiazolate)zinc (**1b**) ($\text{Zn}(4\text{-MeBTZ})_2$): A procedure similar to that for complex **1a** was used to prepare and purify complex **1b**. ^1H NMR (300 MHz, CDCl_3): δ 2.325–2.386(6H, d), 6.556–6.583(2H, d), 6.774–6.834(2H, m), 7.194–7.298(4H, m), 7.421–7.504(2H, m), 7.572–7.661(2H, d), 7.771–7.797(2H, d). Anal. calcd for $\text{C}_{28}\text{H}_{20}\text{N}_2\text{O}_2\text{S}_2\text{Zn}$: C, 61.59; H, 3.69; N, 5.13; found: C, 61.60; H, 3.748; N, 5.076; FT-IR (KBr) cm^{-1} : 3009, 1611, 1536, 1477, 1245, 1205, 1148, 1016, 943, 860, 752.

Bis(2-(5-methyl-2-hydroxyphenyl)benzothiazolate)zinc (**1c**) ($\text{Zn}(5\text{-MeBTZ})_2$): Complex **1c** was synthesized from the reaction between 5-MeBTZ and $\text{Zn}(\text{CH}_3\text{COO})_2 \cdot 2\text{H}_2\text{O}$ in ethanol solution. The mixed solution was stirred for 2 h at room temperature. The precipitate of complex **1c** was obtained, and then purified by vacuum sublimation. ^1H NMR (300 MHz, CDCl_3): δ 2.325(6H,

s), 6.899–6.927(2H, d), 7.172–7.198(8H, m), 7.404–7.430(2H, d), 7.767–7.790(2H, d); Anal. calcd for $\text{C}_{28}\text{H}_{20}\text{N}_2\text{O}_2\text{S}_2\text{Zn}$: C, 61.59; H, 3.69; N, 5.13; found: C, 61.40; H, 3.602; N, 4.562; FT-IR (KBr) cm^{-1} : 3431, 2857, 1620, 1535, 1495, 1444, 1393, 1246, 1187, 982, 823, 724, 707, 591 (Fig. 2).

Bis(2-(hydroxyphenyl)benzothiazolate)zinc (**1**) $\text{Zn}(\text{BTZ})_2$ was synthesized by the reaction between BTZ and $\text{Zn}(\text{CH}_3\text{COO})_2 \cdot 2\text{H}_2\text{O}$ [10].

3. Results and discussion

3.1. Molecular structures

The crystal data, collection information and refinement data for complexes **1a–1c** are summarized in Table 1. The crystal structures are described in Figs. 3a, 4a and 5a, respectively. Selected bond lengths and angles are listed in Table 2. Although the four molecules are in the same crystal system and space groups, their molecular structures have distinct differences. The molecular conformation, molecular packing, bond lengths and bond angles of complex **1** are basically identical to previous reference [10]. Its crystal exists as anhydrous dimer, which consists of two zinc ions with five-coordinate geometry. The Zn(1) and Zn(1A) ions are bridged by two Zn–O bonds (2.017(3) Å), as can be seen in Fig. 2a. The monomer **1b** is four-coordinated by two deprotonated 4-MeBTZ ligand (Fig. 3a). Complexes **1a** and **1c** have two crystallographically independent Zn^{2+} ions, each in distorted four-coordinate geometry, as shown in Figs. 4a and 5a. These peculiar molecular structures are named as bimolecule. Moreover, there is distinct intermolecular π – π interaction between molecules. The steric hindrance provided by the 3-, 4- and 5-methyl groups of phenoxide ring prohibits effectively the formation of pentacoordinate complex.

Though the zinc ions in complex **1** are five-coordinated with distorted trigonal bipyramidal geometry, the Zn(II) ions bearing the methyl-substituted ligands are coordinated by two nitrogen atoms from thiazolate rings and two oxygen atoms from phenoxide rings, forming distorted tetrahedral geometry. The dihedral angles between the phenoxide and benzothiazolate rings in complex **1b** are 2.166° and 3.754°. The dihedral angles including in Zn(1) ion for complex **1a** are 1.194° and 4.280°, while in Zn(2) ion are 4.736° and 1.949°. The dihedral angles between the phenoxide and benzothiazolate rings are 11.702° and 16.626° for the nonbridging ligands for complex **1**, the others are 12.693° and 11.016° for bridging ligands. Therefore, X-ray crystallographic structures have proved that the introduction of methyl led to higher degree of conjugation.

The Zn–N bond lengths are remarkably different, ranging from 1.996(3) Å (Zn(1)–N(1) for complex **1b**) to 2.176 Å (Zn(1)–N(1) for complex **1**). The Zn(1)–O(1) bond length for complex **1** (2.056(3) Å) is significantly longer than that for complex **1b** (1.909(3) Å), complex **1a** (1.919(4) Å) and complex **1c** (1.8951(2) Å). Therefore, introducing methyl group as a substituent on the phenoxide ring effectively enhances the coordination between Zn and N atoms and electrovalent action between Zn and O atoms. The values of bond lengths and angles are changed in bi-molecular structures, suggesting the difference in the coordination effect of zinc in the same complex. For all complexes discussed in this study, Zn–O bonds are shorter than Zn–N bonds. For example, Zn–N lengths of 1.996(3) and 2.023(3) Å are longer than Zn–O lengths of 1.909(3) and 1.898(3) Å in complex **1a**.

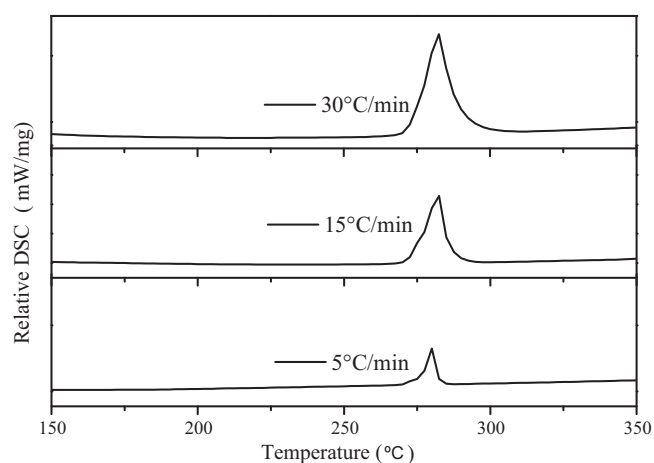
Packing in the solid state depends on the molecular structures of the complexes. Close π – π stacking interactions between adjacent ligands facilitate carrier transport. The π – π stacking of complexes **1** and **1b** occurs in the phenoxide and benzothiazolyl moieties. The aromatic rings between adjacent ligands in complex **1b** are separated with a distance of 3.643 Å. The complex **1a** displays an effective face-to-face overlap between adjacent molecules besides

Table 1
Crystal data and structure refinements for complexes **1a**, **1b** and **1c**.

Identical code	1a	1b	1c
Empirical formula	C ₅₆ H ₄₀ N ₄ O ₄ S ₄ Zn ₂	C ₂₈ H ₂₀ N ₂ O ₂ S ₂ Zn	C ₅₆ H ₄₀ N ₄ O ₄ S ₄ Zn ₂
Formula weight	1091.90	961.95	1091.90
Temperature, K	298(2)	298(2)	293(2)
Wavelength, Å	0.71073	0.71073	0.71073
Crystal system	Triclinic	Triclinic	Triclinic
Space group	<i>P</i> -1	<i>P</i> -1	<i>P</i> -1
Unit cell dimensions			
<i>a</i> , Å	7.7789(9)	8.9899(11)	9.719(2)
<i>b</i> , Å	13.8027(16)	12.1617(15)	11.248(2)
<i>c</i> , Å	23.181(3)	12.8719(16)	11.902(2)
α , deg	104.811(2)	63.492(2)	73.099(3)
β , deg	96.345(2)	84.825(2)	81.498(3)
γ , deg	92.730(2)	71.187(2)	76.476(3)
Volume, Å ³	2384.1(5)	1189.7(3)	1205.8(4)
<i>Z</i>	2	2	11
Density, calcd mg/cm ³	1.521	2.685	2.112
Absorption coefficient, mm ⁻¹	1.235	1.380	5.889
<i>F</i> (000)	1120	976	737
Reflections collected/unique	13287/9048 [R(int)=0.0326]	7503/4529 [R(int)=0.0295]	4385/3838 [R(int)=0.0314]
Data/restraints/parameters	9048/0/635	4529/0/318	3838/0/631
Goodness-of-fit on <i>F</i> ²	0.987	1.066	1.014
Final R indices [<i>I</i> > 2 σ (<i>I</i>)]	R1 = 0.0663, wR2 = 0.1782	R1 = 0.0534, wR2 = 0.1077	R1 = 0.0670, wR2 = 0.1634
R indices (all data)	R1 = 0.1127, wR2 = 0.2304	R1 = 0.0802, wR2 = .1340	R1 = 0.0970, wR2 = 0.2127

initial-to-tail stacking (in Fig. 4c), resulting in a shortest distance of about 3.564 Å. There is also weak S...O interaction besides π - π stacking interactions for complex **1c**, as can be seen in Fig. 5b. On the other hand, complex **1** exhibits a longer intermolecular π - π interaction of 3.7653 Å [10]. The intermolecular π - π interaction has a direct influence on luminescent properties [15,16], discussed below.

To confirm that the single crystal structures are representative of the entire sample, a global optimization method by Rietveld refinement for powder diffraction spectra were carried out. Figs. 3b and 4b reveal that the simulated powder XRD pattern of complex **1b** and **1a** which were calculated from the single crystal data, and the measured powder XRD pattern were practically identical. To further evidence the unique presence of the bi-molecular structure for complex **1a**, the thermal analysis was carried out. From the DSC curves for powder obtained at different heating rates, a single endothermic transition is obtained, which narrows with a decreasing heating rate, as shown in Fig. 6. Simi-

**Fig. 6.** DSC curves of complex **1a** powder at different heating rates.**Table 2**
Experimental structure parameters for complexes **1**, **1a**, **1b** and **1c**.

Complex	1b	1	1a	1c
Bond distances (Å)				
Zn(1)-O(2)	1.898(3)	1.957(3)	1.897(4)	1.8979(2)
Zn(1)-N(1)	1.996(3)	2.176(4)	2.002(5)	2.0149(2)
Zn(1)-O(1)	1.909(3)	2.056(3)	1.919(4)	1.8951(2)
Zn(1)-N(2)	2.023(3)	2.098(4)	2.002(5)	2.0144(2)
Zn(2)-O(4)			1.905(4)	1.957(2)
Zn(2)-O(3)			2.000(7)	1.863(1)
Zn(2)-N(3)			2.007(5)	1.975(1)
Zn(2)-N(4)			2.008(5)	1.985(2)
Bond angles (deg)				
O(2)-Zn(1)-O(1)	127.64(14)	171.89(14)	128.3(2)	117.5(7)
O(2)-Zn(1)-N(2)	93.92(13)	87.36(16)	111.0(2)	89.7(8)
O(1)-Zn(1)-N(2)	107.70(14)	100.16(15)	94.9(2)	132.1(9)
O(2)-Zn(1)-N(1)	115.89(13)	96.77(16)	94.73(19)	123.8(8)
O(1)-Zn(1)-N(1)	94.69(13)	81.98(15)	112.47(18)	92.1(7)
N(2)-Zn(1)-N(1)	118.82(13)	121.33(16)	117.04(19)	104.7(8)
O(4)-Zn(2)-O(3)			127.6(2)	116.5(8)
O(4)-Zn(2)-N(4)			95.2(2)	95.2(7)
O(3)-Zn(2)-N(4)			112.7(3)	122.6(8)
O(4)-Zn(2)-N(3)			113.2(2)	120.5(7)
O(3)-Zn(2)-N(3)			93.9(2)	97.1(6)
N(4)-Zn(2)-N(3)			109.7(2)	106.5(6)

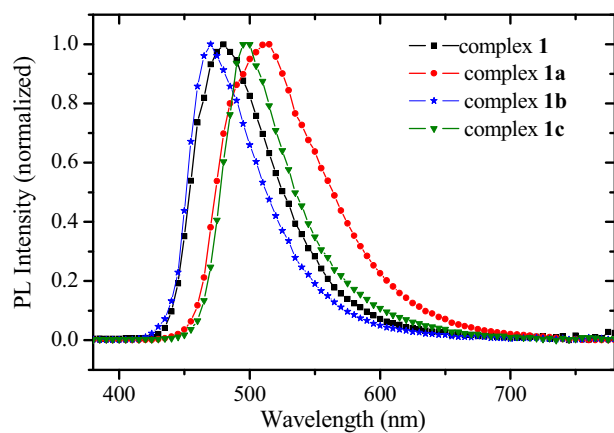


Fig. 7. The PL spectra for thin films of complexes **1**, **1a**, **1b** and **1c**.

lar behavior was observed for complex **1c**. In addition, the ^1H NMR spectroscopy of the single crystal and powder samples in CDCl_3 had identical results. No detectable changes were observed in the FT-IR spectra comparing the single crystal with powder sample dispersed in KBr. These results support the uniqueness in the single crystal and in the powder purified by the vacuum sublimation.

3.2. Thermal stability

Complex **1** exhibits reasonable stability upon exposure to air and high thermal stability. The melting temperature (T_m) and decomposition temperature (T_d) were located at 307 and 500 °C, respectively. Upon methyl substitution, T_m decreases in the order **1c** > **1** > **1b** > **1a**, and T_d decreases in the order **1** > **1b** > **1c** > **1a**. The values T_d of methyl-substituted complexes are lower than that of complexes **1**, indicating that five-coordinate molecular structure results in a higher thermal stability than four-coordinate structures. Thermal analysis results show that **1a** exhibited the lowest T_m and T_d .

3.3. Photophysical properties

The solid-state PL spectra of all complexes can be seen from Fig. 7. Interestingly, complex **1b** has blue-shifted emission relative to other complexes ($\lambda_{\text{max}} = 470$ nm). While the complexes **1a** and **1c** have λ_{max} values at 507 and 499 nm, respectively. Table 3 lists the photophysical data of all complexes. The UV-vis spectra of all complexes exhibit intense absorption bands in the range of 410–430 nm in THF solution, corresponding to the electronic transitions from phenoxide to benzothiazolyl. The absorption bands in 250–380 nm correspond to intraligand transitions [11]. The absorption patterns of all materials are similar in 250–435 nm regions. The maximum absorption bands of **1a** and **1c** appear at lower energies, while complex **1b** occur at much higher energy, as can be seen in Fig. 8.

The results suggest the different substitutional positions of methyl on phenoxide ring can produce different effect on absorp-

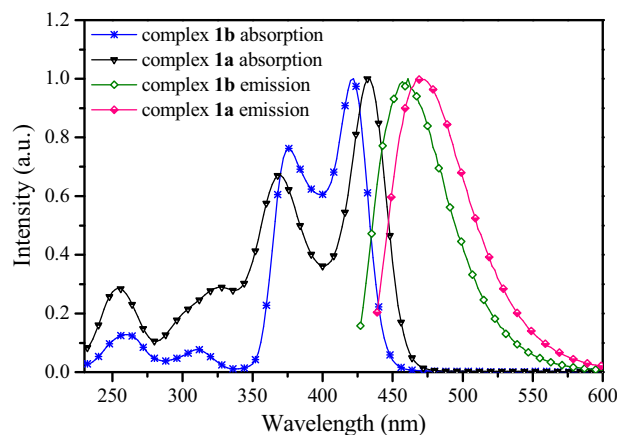


Fig. 8. The absorption and emission spectra of complex **1a** and **1b** in THF solution.

tion spectra. The meta-position substitution to the hydrogen (complex **1b**) results in blue-shift emission and absorption spectra and ortho- (complex **1a**) and para-position (complex **1c**) substitution led to distinct red shift. The optical transition responsible for metal (2-hydroxyphenyl)benzothiazolate complex is centered on the organic ligand [10,12]. This transition is due to a π - π^* charge transfer from the electron rich phenoxide ring (HOMO) to the electron deficient benzothiazolate ring (LUMO). Therefore, observed blue- or red-shifted in absorption and emission spectra can be explained by correlating the electronic effects due to the methyl substituent.

3.4. Electronic structure

To investigate the electronic effects caused by the addition of methyl group, cyclic voltammetry experiments were carried out for all complexes in THF solution. For the electrochemical behavior of all complexes, it has been proposed that the oxidative and reductive processes involve the Zn-phenoxide and -benzothiazolyl moiety. Based on the DFT calculations on monomeric complexes **1b**, the HOMO levels are mostly due to π -orbital contributions from the phenoxide rings, while the LUMO levels are mainly due to the benzothiazolyl rings, as shown in Fig. 9. The experimental data of energy gap, oxidation potentials for all complexes are listed in Table 3. It is evident that all of methyl-substituted complexes show lower oxidative potentials than complex **1**, indicating the relative ease of oxidation. This can be ascribed to the great electro-donating ability of the methyl group. In particular, complexes **1a** and **1c** show lower oxidative potentials than **1b**.

HOMO for complex **1b** has node at 4-positions of the phenoxide rings, and has bonding at 3- or 5-position, but the LUMO has node at 3- or 5-position and has bonding at 4-position. Therefore, complex **1a** and **1c** show obvious decrease in oxidation potential. The reductive potential of complex **1b** was expected to be lower than that of complexes **1a**, **1c**. Theoretical results indicate that complex **1b** has a lower LUMO energy of -3.27 eV compared with complex

Table 3
Photophysical and electrochemical data for complexes (E_m : emission; Φ_{PL} : PL quantum efficiency relative to complex **1** (set to 1); E_{ox} : oxidation potential; Eg: energy gap; τ_{F} : lifetime in THF and voltage: the turn on voltage in the bilayer devices).

Complexes	Absorption (nm)		E_m (λ_{max})		Relative Φ_{PL}	E_{ox} (eV)	Eg (eV)	τ_{F} (ns)	Voltage (V)
	Solution	Powder	Solution	Powder					
1	250, 311, 381, 417	303, 380	466	480	1	1.36	2.32	4.008	9.2
1a	260, 321, 372, 431	322, 414	471	507	0.70	1.28	2.25	3.977	12.7
1b	260, 311, 376, 423	310, 386	460	470	1.56	1.34	2.37	4.724	2.3
1c	252, 318, 384, 417	309, 395	477	496	1.36	1.30	2.28	5.354	10.7

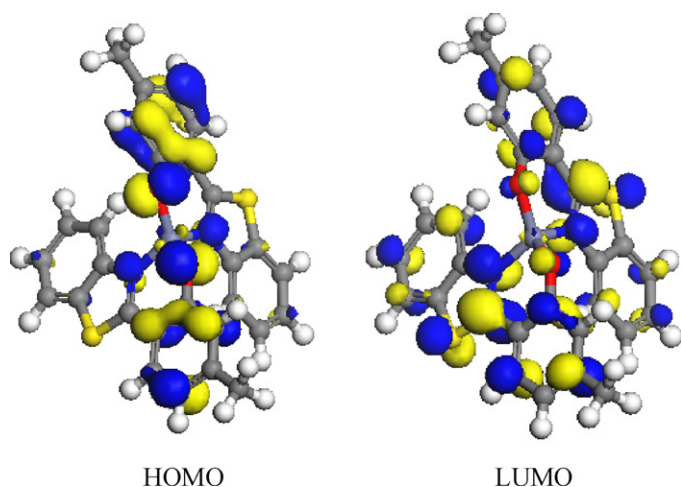


Fig. 9. Molecular orbital population of HOMO and LUMO for complex **1b**.

1 –2.73 eV. The calculated values of HOMO energy is –4.96 eV for complex **1b**.

3.5. Electroluminescent performance

The electroluminescent properties of complexes **1** and **1a–1c** were investigated. The performances of devices were measured using zinc complexes as emitting material and NPB as hole-transport material. The structures of OLEDs used in this work are of typical bilayer, employing ITO as anode and Al as cathode. The λ_{max} of the complexes are in the range of 501–553 nm of EL spectra. No characteristic emission peak of NPB ($\lambda_{\text{max}} = 446$ nm) was observed, indicating that the light emissions originate from emitting materials (in Fig. 10). The EL spectrum of complex **1b** splits into two peaks located at 501 and 544 nm. All the EL spectra have large full width at half maximum (FWHM), e.g. 168 nm for complex **1**, 135 nm for complex **1a**, 110 nm for complex **1b**, and 100 nm for complex **1c**, almost covering the main part of the visible-light range from 420 to 780 nm. The broaden EL spectra relative to PL spectra may be caused by the formation of exciplex at the interface between NPB and Zn complexes [17,18]. The exciplex is a result of charge transfer interaction between the excited state of donor and ground state of acceptor. In this paper, the donor is hole-transfer material (NPB) and the acceptor is emitting-material (Zinc complexes). There is little evidence for exciplex formation in the NPB/Alq bilayer because NPB is a weaker donor [19]. The turn-on voltages (measured at

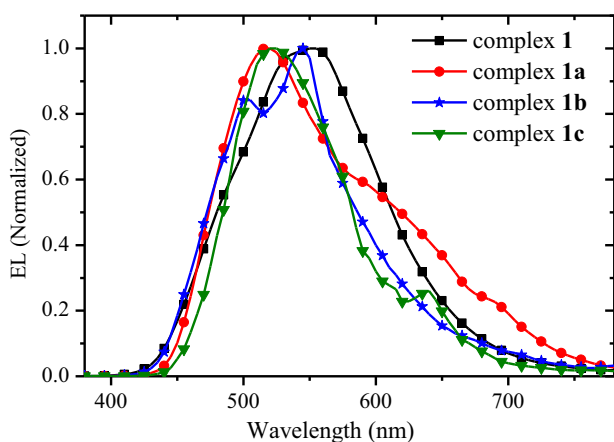


Fig. 10. The EL spectra of all complexes.

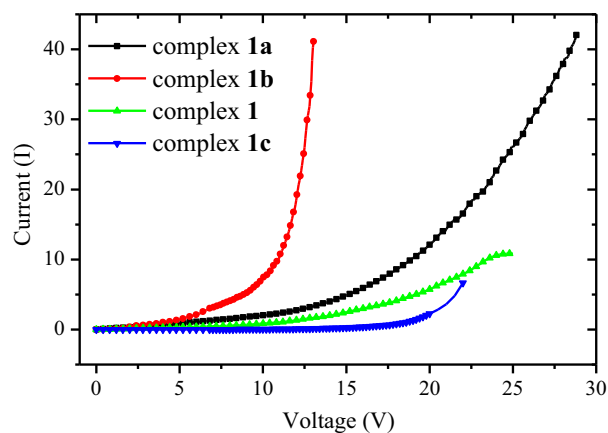


Fig. 11. Current vs voltage plots for all complexes.

1 cd/m²) of complexes **1**, **1a**, **1b** and **1c** are 9.2 V, 12.7 V, 2.3 V and 10.7 V, respectively.

The ability of the emissive layer to trap charges is considered to be the most important factors which determine the operating voltage. The device operating voltage (at a fixed current) increases in the order **1b** < **1a** < **1** < **1c**, as can be seen in Fig. 11. The reason for the higher operating voltages is the poorer carrier-transfer ability at the metal/organic interface. The device based on **1b** has a lower operating voltage.

4. Conclusions

A group of methyl-substituted [Zn(BTZ)₂]₂ derivatives were synthesized, forming dimer monomer, and bi-molecular structures. Their interesting structural features were characterized by single-crystal and powder X-ray diffraction. Lower oxidation potentials of methyl complexes than that of complex **1** were observed, indicating that the methyl group induces a relatively easy oxidation and effective hole trapping. Complex **1b**, which has methyl group at the 4-position of phenoxide, exhibits brighter blue emission, stronger EL intensity, lower turn-on and operating voltages than other complexes. The luminescent mechanisms were discussed with molecular orbital calculations and redox potentials, showing that the luminescent properties are ligand-based and can be tuned by introducing functional groups.

Acknowledgments

This work was financially supported by National Natural Scientific Foundation of China (20671068, 21071108, 60976018); Natural Science Foundation of Shanxi Province (2008011008, 2010021023-2); Program for Changjiang Scholar and Innovation Research Team in University (IRT0972); Innovation Foundation for Graduate Student of Shanxi Province(20081007).

References

- [1] C.W. Tang, S.A. VanSlyke, Appl. Phys. Lett. 51 (1987) 913–915.
- [2] J. An, J. Chang, J. Han, C. Im, Y.-J. Yu, D.H. Choi, J. Jin, T. Majima, J. Photochem. Photobiol. A: Chem. 200 (2008) 371–376.
- [3] S.R. Forrest, Nature 428 (2004) 911–918.
- [4] B.S. Xu, H. Wang, Y.Y. Hao, Z.X. Gao, H.F. Zhou, J. Lumin. 122/123 (2007) 663–666.
- [5] T.T. Wang, G.C. Zeng, H.P. Zeng, P.Y. Liu, R.X. Wang, Z.J. Zhang, Y.L. Xiong, Tetrahedron 65 (2009) 6325–6329.
- [6] H. Xu, Z.F. Xu, Z.Y. Yue, P.F. Yan, B. Wang, L.W. Jia, G.M. Li, W.B. Sun, J.W. Zhang, J. Phys. Chem. C 112 (2008) 15517–15525.
- [7] B.S. Xu, Y.Y. Hao, X.H. Fang, H. Wang, X.G. Liu, Appl. Phys. Lett. 90 (2007) 053903.
- [8] Y. Hamada, T. Sano, H. Fujii, Y. Nishio, H. Takahashi, K. Shibata, Jpn. J. Appl. Phys. 35 (1996) L1339–L1341.

- [9] T. Sano, Y. Nishio, Y. Hamada, H. Takahashi, T. Usuki, K. Shibata, J. Mater. Chem. 10 (2000) 157–161.
- [10] G. Yu, S.W. Yin, Y.Q. Liu, Z.G. Shuai, D.B. Zhu, J. Am. Chem. Soc. 125 (2003) 14816–14824.
- [11] Y.P. Tong, S.L. Zheng, X.M. Chen, Inorg. Chem. 44 (2005) 4270–4275.
- [12] B.S. Xu, H.X. Xu, X.H. Fang, L.Q. Chen, H. Wang, X.G. Liu, Org. Electron. 9 (2008) 906–910.
- [13] H.J. Son, W.S. Han, J.Y. Chun, B.K. Kang, S.N. Kwon, J. Ko, S.J. Han, C. Lee, S.J. Kim, S.O. Kang, Inorg. Chem. 47 (2008) 5666–5676.
- [14] Y. Kan, G.S. Wu, L.D. Wang, Y. Qiu, Int. J. Quantum Chem. 98 (2004) 325.
- [15] S. Jung, Y. Kang, H.S. Kim, Y.H. Kim, C.L. Lee, J.J. Kim, S.K. Lee, S.K. Kwon, Eur. J. Inorg. Chem. (2004) 3415–3423.
- [16] V.V. Grushin, N. Herron, D.D. LeCloux, W.J. Marshal, V.A. Petrov, Y. Wang, Chem. Commun. (2001) 1494–1495.
- [17] X. Xu, Y. Liao, G. Yu, H. You, C.A. Di, Z.S. Su, D.G. Ma, Q. Wang, S.Y. Li, S.Q. Wang, J.P. Ye, Y.Q. Liu, Chem. Mater. 19 (2007) 1740–1748.
- [18] S.P. Singh, Y.N. Mohapatra, M. Qureshi, S.S. Manoharan, Appl. Phys. Lett. 86 (2005) 113505.
- [19] H. Wang, K.P. Klubek, C.W. Tang, Appl. Phys. Lett. 93 (2008) 093306.